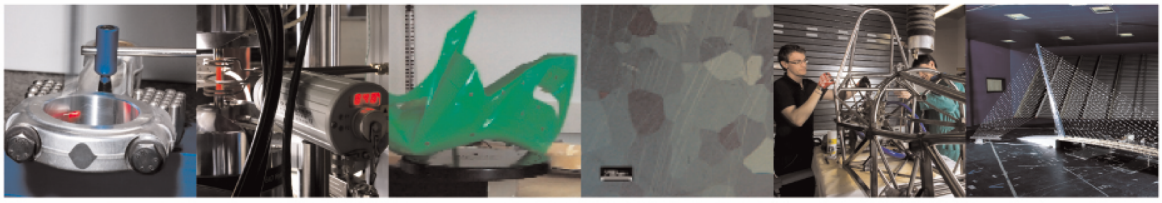

Load Interaction Effects in Propagation Lifetime and Inspections of Railway Axles

S. Beretta, M. Carboni, D. Regazzi

This is a post-peer-review, pre-copyedit version of an article published in International Journal of Fatigue. The final authenticated version is available online at:
http://dx.doi.org/10.1016/j.ijfatigue.2016.03.009

DIPARTIMENTO DI MECCANICA ■ POLITECNICO DI MILANO
via G. La Masa, 1 ■ 20156 Milano ■ EMAIL (PEC): pecmecc@cert.polimi.it
http://www.mecc.polimi.it
Rev. 0

Load Interaction Effects in Propagation Lifetime and Inspections of Railway Axles

S. Beretta*, M. Carboni, D. Regazzi

Politecnico di Milano, Dipartimento di Meccanica, Via La Masa 1, 20156 Milano (IT)

Abstract

As well known, an interaction effect arises, on crack propagation, when a specimen or a component is subjected to variable amplitude fatigue loading. Depending on the applied load sequence, a certain amount of retardation or acceleration can then be observed, on the fatigue crack growth rate, with respect to the constant amplitude case. In the case of structural ductile materials, the interaction phenomenon is mainly addressed by the local plasticity at the crack tip and can be explained, from a global point of view, by adopting the crack closure concept. In the present research, load interaction effects in a medium strength steel for railway axles are experimentally analyzed by companion and full-scale specimens. The experimental outcomes show a significant retardation with respect to a simple no-interaction approach and the Strip-Yield model offers good, yet conservative, estimates of crack advance. The consequences of crack growth retardation on the inspection periodicity of railway axles are then discussed.

Keywords: crack propagation, variable amplitude loading, railway axles, inspection intervals, medium strength axle steel

1. INTRODUCTION

Railway axles are usually designed against fatigue limit [1, 2], but, due to their very long service life (30 years or even more on European lines) and to in-service damage like corrosion or ballast impacts, the approach has moved to damage tolerance [3, 4, 5]. From this point of view, the presence of cracks in axles is accepted and they must be periodically inspected using non-destructive techniques. The problem so moves to the determination of the appropriate maintenance inspection intervals, based on crack growth life predictions and the

*Corresponding author
Email address: stefano.beretta@polimi.it (S. Beretta)

adopted non-destructive testing technique [6]. Considering the former aspect of inspection intervals, it is well known from the literature that an interaction effect on crack propagation arises when a specimen or a component is subjected to variable amplitude (VA) fatigue loading, like railway axles. Depending on the applied load sequence, a certain amount of retardation or acceleration in fatigue crack growth rate can then be observed if compared to the constant amplitude (CA) loading case. In the case of structural ductile materials, this interaction phenomenon is mainly addressed by the local plasticity at the crack tip and can be explained, from a global point of view, by adopting the 'plasticity-induced crack closure' concept [7, 8].

In the case of railway axles, apart the numerical simulations in [9], the papers with experimental VA tests show that: i) at relatively high stresses (higher that the ones adopted for axle design) there is absence of load retardation [10, 11]; ii) under realistic stress spectra, there is a significant retardation for both a normalized C45 steel grade [12] and a quenched and tempered 25CrMo4 grade and higher grades [11, 13]. As for the axles, it has to be remarked than the present test apparatuses for full-scale axles (three point bending [10, 12] , cantilever bending [11, 14] or wheel-roller [13]) do not allow to make tests with real stress histories, but they can only apply sequences of block loadings. The effect of this simplification has not been yet thoroughly investigated.

The present paper aims at complementing the previous results about VA effects onto crack propagation in railway axles by a series of analyses (experiments and simulations) on the standardized medium strength EA4T grade [15], a quenched and tempered 25CrMo4 grade. VA tests were performed on SE(T) companion specimens and crack propagation was experimentally measured considering the original in-service load time history and different equivalent block loading sequences defined from it. An experimental full-scale test under block loading was carried out, as well. Eventually, crack growth predictions, using both a simple no-interaction algorithm and a Strip-Yield model [16], were carried out for small-scale and full-scale specimens and compared to experimental

evidence. The effect of the significant crack retardation onto inspection intervals of railway axles is then discussed.

2. Experiments

2.1. Crack growth behaviour of EA4T steel grade

A dedicated experimental campaign was carried out, for each batch, in order to investigate the crack propagation behavior of the EA4T grade at constant amplitude loading. The near-threshold region was particularly investigated, because, typically, the life of a railway axle is mostly spent within such a region. The details about this campaign are reported in [17], while a summary is provided in the following. Eight traditional SE(B) specimens from batch A and twelve from batch B, all having a 12x24 mm^2 cross section and an 8 mm initial notch length obtained by electro-discharge machining (EDM), were tested. Each specimen was pre-cracked under compression. Crack propagation tests onto SE(B) specimens were then carried out using a Rumul Craktronic resonant plane bending facility having a capacity equal to 160 Nm and working at a frequency of about 130 Hz. Crack length was measured, on either side of the crack, using 10 mm crack-gages and a dedicated control unit, by the potential drop technique. Specimens were tested at different stress ratios ranging from $R = 0.7$ to $R = -2.5$.

2.2. Variable amplitude loading experiments on SE(T) companion specimens

A new type of SE(T) specimen (width equal to 50 mm, thickness equal to 20 mm and initial notch length equal to 6 mm, as in Figure 1(a)), having the same crack tip 'constraint' of cracks in real axles, was adopted for variable amplitude loading experiments as a companion specimen of full-scale axles [18] . Tests were performed by a mono-axial servo-hydraulic Schenck facility with 250 kN maximum load. First, specimens were pre-cracked under compression, in order to obtain, similarly to small-scale SE(B) specimens, a non-propagating and naturally arrested fatigue crack characterized by no closure effects, as in

the example of Figure 1(b). After compression pre-cracking, each specimen was instrumented by two 20 mm crack-gages, one on either side, for real-time crack length monitoring by a potential drop technique. Moreover, before starting each test, eight strain gages were glued on each specimen in order to verify the correct alignment of the load axis: the SE(T) specimen equipped for tests is shown in Figure 1(c).

The complete plan of VA experiments on SE(T) specimens is shown in Table 1. The first two SE(T) specimens (EA4T batch B steel grade) were tested with the aim to check the crack propagation behavior of the material subjected to a load-time history and to an equivalent block load sequence derived from the time history itself. These experiments were also performed because the typical fatigue test machines used for testing full-scale axles are not able to apply load time histories, but only block load sequences and the possible differences in the response could then be checked. The applied load-time history is representative of 57000 km of service and was derived by in-service measurements onto a high-speed train. Figure 2(a) shows the load spectrum of the load-time history and compares it to its equivalent block loads: the blocks were rearranged according to a Gassner sequence [19] typically adopted by some European railway operators for the homologation of axles and here defined as 'long blocks' sequence (Figure 2(b)). The amplitudes of both the load-time history and the block load sequence were applied to specimens after being scaled so that their maximum ΔK_{max} at the beginning of each test was equal to the one at the tip of a 2.5 mm deep crack located in the most stressed section along the groove of a real axle.

2.3. Variable amplitude loading full-scale test

A full-scale railway axle was tested using the 'long blocks' sequence. The full-scale specimen, shown in Figure 3(a) and made of EA4T batch B steel grade, was tested under three point rotating bending on a dedicated fatigue test machine, available at the Department Mechanical Engineering - Politecnico di Milano, having a capacity of 250 kNm and a rotational speed of about 9 Hz.

The static scheme of the test machine is shown in Figure 3(b). Two artificial notches were machined at the section highlighted in Figure 3(a) by EDM, at 180 from each other, in order not to interfere during crack propagation. The notches had a semi-elliptical shape, with initial depth $a_0 = 1.5$ mm and aspect ratio $a/c = 0.67$, according to Figure 3(c). The full-scale specimen was first subjected to 10 repetitions of the 'long blocks' sequence scaled to a maximum SIF value equal to the one applied to SE(T) specimens, in order to initiate a sharp crack out of the artificial notches. Then, other 90 repetitions were applied and, finally, since no significant crack advance was measured, to another 77 repetitions increasing the load levels of the 'long blocks' sequence by 25%.

3. Results

3.1. Constant amplitude loading tests

Figure 4(a) shows the experimental CA crack growth curves obtained from each batch, along with their interpolation carried out applying the maximum likelihood method to Forman-Mettu's equation for crack growth rates [20]:

$$\frac{da}{dN} = C\left[\left(\frac{1-f}{1-R}\right)\Delta K\right]^n \frac{\left(1-\frac{\Delta K_{th}}{\Delta K}\right)^p}{\left(1-\frac{K_{max}}{K_c}\right)^q} \tag{1}$$

where C, n, p and q are the empirical constants, ΔK_{th} is the threshold SIF range, K_{max} and K_c are the maximum and the critical SIF values, respectively, R is the stress ratio and f is the 'Newman's closure function' [16] describing the plasticity-induced crack closure phenomenon:

$$f = \frac{S_{op}}{S_{max}} = \begin{cases} \max\left(R, A_0 + A_1 R + A_2 R^2 + A_3 R^3\right) & R \geq 0 \\ A_0 + A_1 R & -2 \leq R < 0 \end{cases} \tag{2}$$

where S_{op} is the opening stress. The involved coefficients are defined as [16]:

$$\begin{aligned} A_0 &= \left(0.825 - 0.34\alpha + 0.05\alpha^2\right)\left[\cos\left(\frac{\pi S_{max}}{2\sigma_y}\right)\right]^{\frac{1}{\alpha}} \\ A_1 &= \left(0.415 - 0.071\alpha\right)\frac{S_{max}}{\sigma_y} \\ A_2 &= 1 - A_0 - A_1 - A_3 \\ A_3 &= 2A_0 + A_1 - 1 \end{aligned} \tag{3}$$

being α the 'constraint factor' originally proposed [16] by Newman as the calibrating parameter of the Strip Yield model. $\frac{S_{max}}{\sigma_y}$ is, instead, the ratio between the maximum applied stress and the cyclic yield one.

In Figure 4(a), data were normalized due to their proprietary nature. In spite of the big differences between the two experimental approaches considered for characterizing the threshold region, the two data sets are in good agreement in the linear region of the da/dN-ΔK diagram, as previously shown by the authors [21] for EA4T and EA1N steel grades.

Figure 4(b) shows (normalized again) the trend of thresholds as a function of stress ratio R, as derived from the current experimental campaigns, and compares it to data available in the literature [22] and obtained by the ΔK-decreasing technique (batch B only). The same figure also shows the interpolation of experimental data, applying the maximum likelihood method to Forman-Mettu's equation for thresholds [20]:

$$\Delta K_{th} = \Delta K_{th0}\frac{\sqrt{\dfrac{a}{a+a_0}}}{\left[\dfrac{1-f}{(1-A_0)(1-R)}\right]^{(1+C_{th}R)}} \tag{4}$$

where A_0 is described in Eq. (3), ΔK_0 is the threshold value at $R = 0$, C_{th} is an empirical constant, a is the crack length and a_0 is the El-Haddad parameter [23]. The dependence of ΔK_{th} on R is controlled through the C_{th} parameter: different values of C_{th} (namely C_{th}^{+} and C_{th}^{-}) have to be considered for positives and negatives R-values. The empirical parameters, determined by interpolating

experimental data, were then ΔK_0, C^+_{th} and C^-_{th}: it is evident that the compression pre-cracking technique results in lower thresholds when compared to the traditional approach, especially considering the lowest stress ratios. This is in accordance to what was found for EA1N steel [22]. The threshold trend line of EA4T batch A is instead higher over the whole stress ratio range, as shown in Figure 4(b). Since it was not possible to carry out threshold experiments on EA4T batch A steel grade adopting the ΔK-decreasing methodology, the increase of ΔK_{th} at $R = -1$ was estimated, for prospective crack growth simulations adopting the threshold trend by ΔK-decreasing, to be approximately 15%, as for EA4T batch B data.

3.2. Variable amplitude loading tests on companion specimens

Figure 5(a) directly compares the crack advance Δa registered during the two tests. As can be seen, they seem comparable, at least over the initial propagation of the crack. It is also worth adding such a crack advance was considered, for both tests, starting from the stabilization of the closure level, as shown in Figures 5(b) and 5(c). In particular, after the stabilization, the experimental $U = \Delta K_{eff}/\Delta K$ value resulted to be about 0.35 for both tests, in accordance to the indications given by Schijve [24] for $R = -1$.

Regarding the tests carried out onto EA4T batch A steel grade, the load spectrum was amplified, compared to specimens from batch B, by 25%, and the mean stress shown in Figure 2(a) was also considered. This mean stress value was added to each block of the discretized load spectrum and the blocks were then rearranged in the already adopted Gassner sequence, obtaining the 'long blocks' load sequence shown, again normalized, in Figure 2(b). It is worth noticing that, due to the superposition of the constant stress value onto the load spectrum, the resulting stress ratio moves from the typical value $R = -1$ (pure rotating bending), to less negative values. The acting stress ratios are between zero and minus one. Since the aim of this research was to understand the effect of block length onto crack propagation, two different lengths were adopted: the already described 'long blocks' load sequence (upper plot in Figure

2(b)), composed of about 5 million cycles, and a 'short blocks' one, obtained dividing the number of cycles of each block by seven (lower plot in Figure 2(b)). Specimen A4T-SE(T)#1 was tested applying the 'long blocks' load sequence, while specimen A4T-SE(T)#2 was tested using the 'short blocks' one. Results of crack propagation on the two tested specimens, both from batch A, are shown in Figure 6(a).

Crack closure levels, recorded during the tests, are shown in Figures 6(b) and 6(c). As can be seen, they are higher than expected: the two red dotted lines, representing the extreme values according to Schijve's formulation [24] at the involved stress ratios, are lower than the experimental outcomes, which, anyway, showed comparable trends. This behavior appears to be due to the fact that, at lower stress amplitudes when crack advance is negligible, S_{op} values remain 'frozen' at the values of the higher stress amplitudes, where a sudden crack advance happens causing a 'large opening' of the crack tip. This closure level should indicate a faster crack growth, while, actually, the crack does not propagate at all during the lower load levels, due to the crack tip plasticity induced by the higher ones.

3.3. Variable amplitude loading test on full-scale specimen

Crack growth was monitored, during the test, by means of plastic replicas and an optical microscope, aimed at measuring the increase of crack length at surface (c in Figure 3(b)). An example of surface crack advance, at one side of one of the initial notches, is shown in Figure 7. Crack depth was estimated from the measured surface length by means of the following expression suggested in the literature [25]:

$$a = \frac{D}{2} \cdot (1 + \tan\theta - \sec\theta) \quad \text{with} \quad \theta = \frac{2c}{D} \tag{5}$$

where $2c$ is the total crack length and D is the diameter of the axle body. The validity Eq. 5 was previously checked by the authors [10] comparing the estimated shape with the one predicted by the NASGRO software. At the end

of the test, cracks developed almost equally at the two micronotches; for this reason, crack depth for comparison with simulations is taken as the mean value between the two monitored cracks. A total crack advance less than 0.3 mm was measured during the 190 load spectrum repetitions. Details of crack propagation results will be shown in Sec. 4.2 together with crack growth simulations.

4. Analysis

4.1. Companion specimens

Crack growth simulations were initially carried out using a simple no-interaction model, adopting both compression pre-cracking and ΔK-decreasing thresholds, in order to quantify how much the experimental methodology for the definition of the thresholds can affect predictions. A first result, clearly appearing in Figures 8 and 9, is that, for all the tested specimens, the experimental outcomes always lie in between no-interaction simulations performed by either compression pre-cracking or ΔK-decreasing methodologies. In particular, adopting compression pre-cracking parameters, simulations always result in conservative predictions, while, on the contrary, they result in non-conservative predictions when adopting ΔK-decreasing parameters. It is worth remarking that:

- the adoption of ΔK*-decreasing* would have led to the wrong idea that the crack *accelerates* with respect to no-interaction simulations;
- the adoption of CPLR crack growth returns the correct evaluation that cracks are subjected to retardation.

Then, a more refined attempt to match lifetime predictions to the experiments consisted in the use of the Strip-Yield model, as implemented in the commercial software Nasgro v. 4.23 [25]. By the Strip-Yield model, it is possible to take into account for interaction effects, during propagation, due to crack tip plasticity and the consequent crack closure. The experimental effective crack growth curve (conventionally taken at $R = 0.7$) of each batch of EA4T steel grade, derived from the compression pre-cracking experimental methodology,

was provided as an input for material modeling. The constraint factor values for strip yield simulations were set, for both batches, to $\alpha = 2.5$, according to Nasgro user's manual [25] for the case of steels. Nevertheless, this assumption was verified by CA crack growth simulations at stress ratio $R = -1$ (Fig. 4(a)), returning in a good description of crack growth curves onto SE(T) specimens [17, 26], confirming the validity of the chosen α value.

The conclusion that can be drawn is that, regarding the tests under variable amplitude loading, a slight retardation appears, due to the interaction between load levels, and this can be well represented by the Strip-Yield model. Moreover, the amount of retardation does not depend very much on the type of applied load sequence.

4.2. Full-scale specimen

Results of crack propagation onto the full-scale specimen are shown in Figure 10. About 16 repetitions of the block load sequence were required for crack closure stabilization, as clearly visible from the initial behavior of the experimental curve. A series of simulations were carried out considering the no-interaction model and the SY one from the crack depth after stabilization.

As can be seen in Figure 10, both models overestimate the growth rate. However, the no-interaction model would predict a crack advance of 2 mm in approx. 170 sequences (failure is predicted to occur within 190 sequences), while the SY one would predict a stable crack advance of 0.6 mm. It is worth mentioning that the SY simulation show approximately the same constant growth rate observed on the full-scale axle, during the 100% stress spectrum, while when the stress amplitudes are increased to 125% the growth rate is overstimated approximately by a factor of 2.

5. Discussion on inspection intervals

The conclusion that can be drawn from the experiments is that no-interaction calculations are too conservative for the estimation of crack growth under service conditions. It is important to annotate that a significant retardation has

been also observed by Mädler et. al. [13] as a result of VA crack growth tests on A4T axles: also in that paper, the authors have reached the conclusion that it is necessary to include retardation effects in the calculation of axle propagation lifetime. On the other hand, present results on SE(T) specimens and a full-scale axle have validated the application of SY simulations to EA4T steel.

Now, given a trustful fatigue crack growth calculation, the most suitable inspection interval, leading to a trade-off between total life cycle costs and absolute safety, can be determined keeping in mind that the number of inspections, carried out during the in-service axle life, directly influences the probability of failure of the axle itself. From this point of view, given the length L of the inspection interval, the total cumulative probability of detection (PC_{DET}) of a propagating crack can be calculated [27] (Fig. 11(a)) using the 'Probability of Detection' (POD) curve [28] of the adopted NDT technique at each i^{th} inspection, at which crack size equals a_i, before failure. Figure 11(b), where three possible inspections are assumed before failure, shows this approach. The PC_{DET} value can then be quantified as:

$$PC_{DET} = 1 - \left[\prod_i POND\,(a_i)\right] = 1 - \left\{\prod_i \left[1 - POD\,(a_i)\right]\right\} \qquad (6)$$

where $POND(a)_i$ ('Probability of Non Detection') represents the probability to fail the i^{th} detection. The drawback of this approach is that the repetition of inspections on small cracks having very low POD (i.e. during the initial s of propagation life) increases PC_{DET}, but introduces further influences (sizing errors, human factors, ...) typical of this stage, so focusing again the attention on the best trade-off between safety and costs.

It is then worth comparing the prospective inspection intervals to be applied to a prospective axle, made of EA4T, with a diameter $D = 160$ mm and an initial 1 mm deep crack a_o subjected to three different in-service load spectra for high speed trains. The three load spectra considered were: i) spectrum A adopted for VA tests; ii) the HYPERWHEEL load spectrum for an intercity train derived from Fischer and Grubisic [29]; iii) the WIDEM test spectrum

[12]. The three spectra, compared in Fig. 12, have been discretized for the simulations considering the same maximum stress amplitude of 200 MPa. Crack propagation lifetime has been calculated by no-interaction and SY models, while the inspection interval has been calculated so that the *total cumulative probability of non-detection* is 10^{-5} adopting a *Near End Scan* ultrasonic inspection [27].

Results, shown in Table 2, show that the adoption of a crack growth interaction analysis (based on the here-validated SY analyses) would allow to obtain life predictions 6 times longer than the ones with *no-interaction model*. Moreover, the increase of the inspection intervals, with respect to those calculated by a simple no-interaction approach, it is approximately a factor of 8 due to the less steep crack growth rate. The conclusion that can be drawn is that it is then important to include retardation effects into the determination of inspection intervals.

6. Concluding remarks

Load interaction effects in propagation lifetime of railway axles, made of EA4T steel grade, were studied and analysed both experimentally and numerically. Main results can be summarized:

- the growth rate of two batches of EA4T steel have been experimentally obtained by CPLR technique;
- no evidence of an interaction effect arose in terms of the shape of the applied VA loading, for both batches: results derived applying a load-time history versus an equivalent block load sequence, or long blocks versus short ones, are always in good agreement; this allows the application of block load sequences to full-scale specimens (where it is not feasible to apply a load-time history) without affecting results;
- the experimental evidence is always in between no-interaction simulations

adopting thresholds obtained by either compression pre-cracking (conservative predictions) or ΔK-decreasing (non-conservative predictions);

- an evident retardation effect clearly appears, with respect to no-interaction predictions adopting compression pre-cracking thresholds; such a retardation effect was justified and quantified by the performed strip yield simulations;
- the same results, obtained by companion specimens, were observed by a full-scale specimen subjected to the same block load sequence and the simulations of the full-scale test;
- the adoption of SY simulations would allow a significant extension of inspection intervals with respect to periodicities calculated by the no-interaction model.

References

[1] UNI-EN13103, Railway applications - wheelsets and bogies - non powered axles - design method, UNI EN 13103:2012, UNI - Ente Nazionale Italiano di Unificazione, Milano, Italy (2012).

[2] UNI-EN13104, Railway applications - wheelsets and bogies - powered axles - design method, UNI EN 13104:2012, UNI - Ente Nazionale Italiano di Unificazione, Milano, Italy (2012).

[3] A. Grandt, Fundamentals of structural integrity: damage tolerant design and nondestructive evaluation, John Wiley Hoboken, New Jersey, 2004.

[4] U. Zerbst, R. Lundén, K. Edel, R. Smith, Introduction to the damage tolerance behaviour of railway rails–a review, Engineering fracture mechanics 76 (17) (2009) 2563–2601.

[5] S. Cantini, S. e. Beretta, Structural reliability assessment of railway axles, LRS-Techno Series 4, 2011.

[6] S. Cantini, S. Beretta, M. Carboni, POD and inspection intervals of high speed railway axles, in: Proc. 15 th Int. Wheelset Congress, 2007.

[7] J. Schijve, Fatigue crack propagation in light alloy sheet material and structures, NLL, 1960.

[8] J. Bannantine, J. Comer, J. Handrock, Fundamentals of metal fatigue analysis, Vol. 90, Prentice Hall Englewood Cliffs, NJ, 1990.

[9] U. Zerbst, M. Schödel, H. T. Beier, Parameters affecting the damage tolerance behaviour of railway axles, Engineering Fracture Mechanics 78 (5) (2011) 793–809.

[10] S. Beretta, M. Carboni, Simulation of fatigue crack propagation in railway axles, in: Fatigue and Fracture Mechanics, 34th Volume, ASTM International, 2005.

[11] M. Luke, I. Varfolomeev, K. Lütkepohl, A. Esderts, Fatigue crack growth in railway axles: assessment concept and validation tests, Engineering Fracture Mechanics 78 (5) (2011) 714–730.

[12] S. Beretta, M. Carboni, Variable amplitude fatigue crack growth in a mild steel for railway axles: experiments and predictive models, Engineering Fracture Mechanics 78 (5) (2011) 848–862.

[13] K. Maedler, T. Geburtig, D. Ullrich, An experimental approach to determining the residual lifetimes of wheelset axles on a full-scale wheel-rail roller test rig, Int. J. Fatigue 86 (2016) 58–63.

[14] M. Traupe, S. Jenne, K. Lütkepohl, I. Varfolomeev, Experimental validation of inspection intervals for railway axles accompanying the engineering process, International Journal of Fatigue 86 (2016) 44–51.

[15] UNI-EN13261, Railway applications - wheelsets and bogies - axles - product requirements, UNI EN 13261:2011, UNI - Ente Nazionale Italiano di Unificazione, Milano, Italy (2011).

[16] J. Newman, A crack opening stress equation for fatigue crack growth, International Journal of Fracture 24 (4) (1984) R131–R135.

[17] S. Beretta, M. Carboni, D. Regazzi, Load interaction effects in a medium strength steel for railway axles, in: Jacksonville, Florida, 13-15 November 2013, ASTM International, 2013.

[18] M. Carboni, S. Beretta, M. Madia, Analysis of crack growth at R=-1 under variable amplitude loading on a steel for railway axles, J ASTM Int 5 (7).

[19] E. Gaßner, Auswirkung betriebsähnlicher belastungsfolgen auf die festigkeit von flugzeugbauteilen, Jahrbuch deutsch. Luftfahrtforschung (1941) 472–483.

[20] R. Forman, S. Mettu, Behavior of surface and corner cracks subjected to tensile and bending loads in ti-6al-4v alloy, Tech. rep., National Aeronautics and Space Administration, Houston, TX (USA). Lyndon B. Johnson Space Center (1990).

[21] M. Carboni, D. Regazzi, Effect of the experimental technique onto R dependence of ΔK_{th}, Procedia Engineering 10 (2011) 2937–2942.

[22] M. Carboni, L. Patriarca, D. Regazzi, Determination of ΔK_{th} by compression pre-cracking in a structural steel, J ASTM Int 6 (9) (2009) 1–13.

[23] E. HADDAD, et al., Fatigue crack propagation of short cracks, Trans. ASME J. Eng. Mater. Technol. 110 (1979) 42–46.

[24] J. Schijve, Some formulas for the crack opening stress level, Engineering Fracture Mechanics 14 (3) (1981) 461–465.

[25] N. J. S. Center, Fatigue crack growth computer program NASGRO version 4.2-Reference manual (2006).

[26] D. Regazzi, Advances in life prediction and durability of railway axles, Ph.D. thesis, Politecnico di Milano (2014).

[27] M. Carboni, S. Beretta, Effect of probability of detection upon the definition of inspection intervals of railway axles, IMechE, Part F: J. Rail Rapid Transit 221 (2007) 409–417.

[28] G. Georgiou, Probability of detection (pod) curves: derivation, applications and limitations, Tech. rep., HSE Books, Health and Safety, Executive (2006).

[29] G. Fisher, V. Grubisic, Bemessung von Radsatzwellen – Einflussgrssen und Vorgehen bei der Auslegung, Bericht FB-226, Fraunhofer LBF, Darmstadt (2005).

Specimen	Batch	VA loading	S_{max}/S_{y-cyc}	$\Delta K_{max}/\Delta K_{th}$
A4T-SE(T)#1	A	Long blocks ($R \neq -1$)	0.21	2.0
A4T-SE(T)#2	A	Short blocks ($R \neq -1$)	0.21	2.0
A4T2-SE(T)#4	B	Time history ($R = -1$)	0.20	1.2
A4T2-SE(T)#5	B	Block loading ($R = -1$)	0.20	1.2

Table 1: Summary of VA experiments on SE(T) specimens

	no-interaction		SY simulations	
	normalized life	inspection interval	normalized life	inspection interval
Spectrum A (Fig. 3)	1	0.14	6.33	1.05
Spectrum B - HYPERWHEEL	1	0.11	7.93	1.30
Spectrum C - WIDEM	1	0.16	5.90	0.85

Table 2: Normalized propagation lifetimes and inspection intervals on a prospective axle made of EA4T ($D = 160\,mm$, initial crack depth $a_o = 1\,mm$, maximum stress amplitude $S_{\max} = 200\,MPa$)

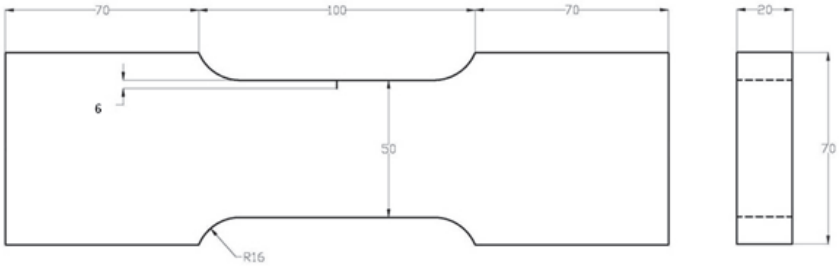

(a)

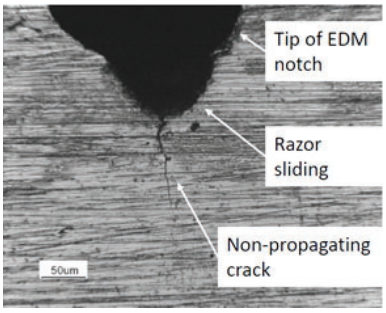

(b)

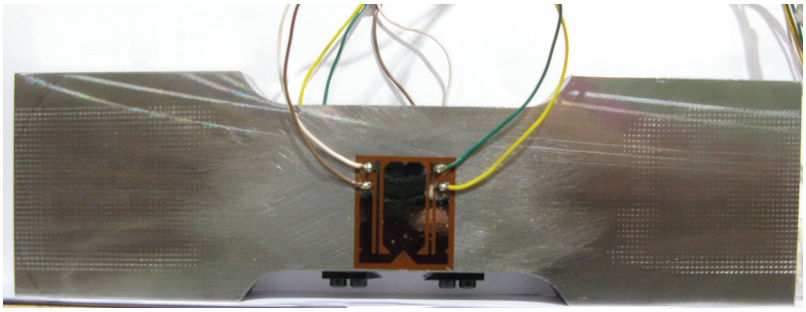

(c)

Figure 1: Experimental set-up for variable amplitude loading tests: a) geometry of the adopted SE(T) specimen; b) example of generated non-propagating and closure-free crack after 'razor sliding' and compression pre-cracking: final length equal to 0.096 mm; c) detail of a specimen instrumented by crack-gages and clip-gage.

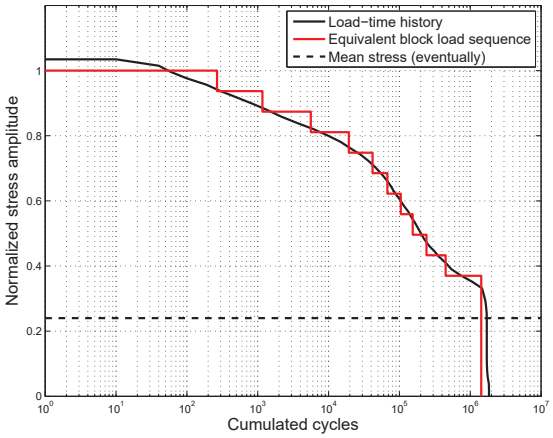

(a)

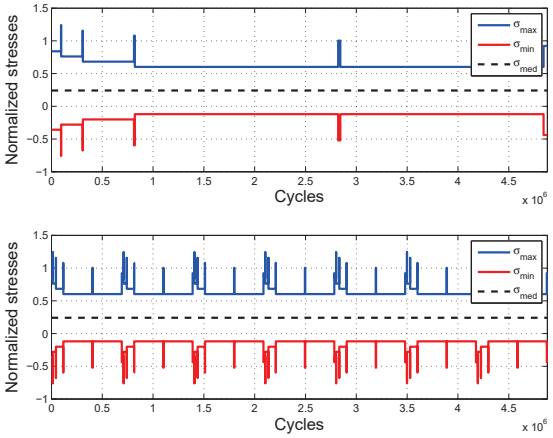

(b)

Figure 2: Normalized variable amplitude loadings derived from in-service measurements: a) in-service stress spectrum and its equivalent block load discretization; b) adopted Gassner block load sequences ($R \neq 1$): 'long blocks' (upper figure) against 'short blocks' (lower figure).

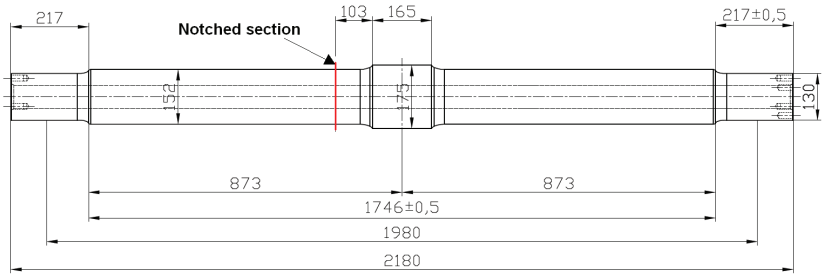

(a)

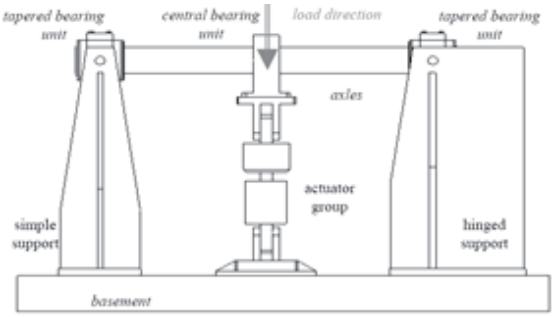

(b)

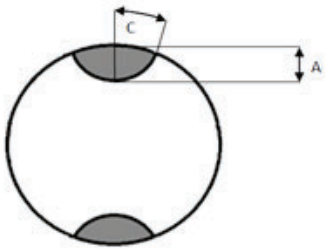

(c)

Figure 3: Experimental set-up for variable amplitude loading full-scale test: a) drawing of the specimen; b) schematics of the three point rotating bending facility; c) notches by EDM in the highlighted section.

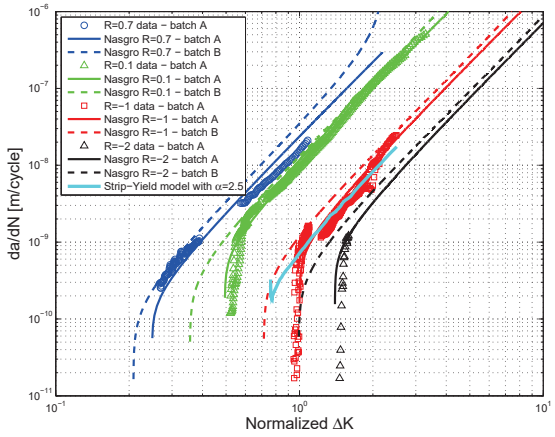

(a)

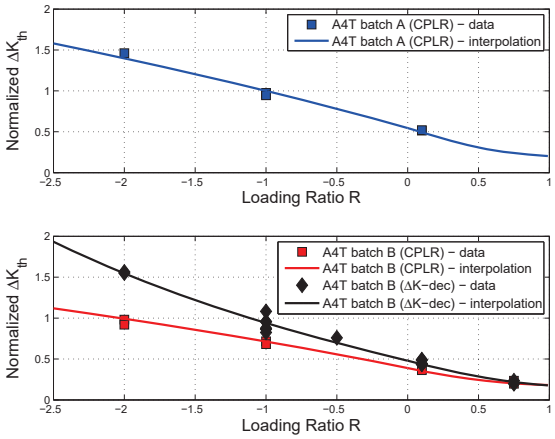

(b)

Figure 4: Constant amplitude crack growth characterisation of the considered EA4T steel: a) crack growth curves and interpolation with Nasgro equation; b) dependence of thresholds on stress ratio R.

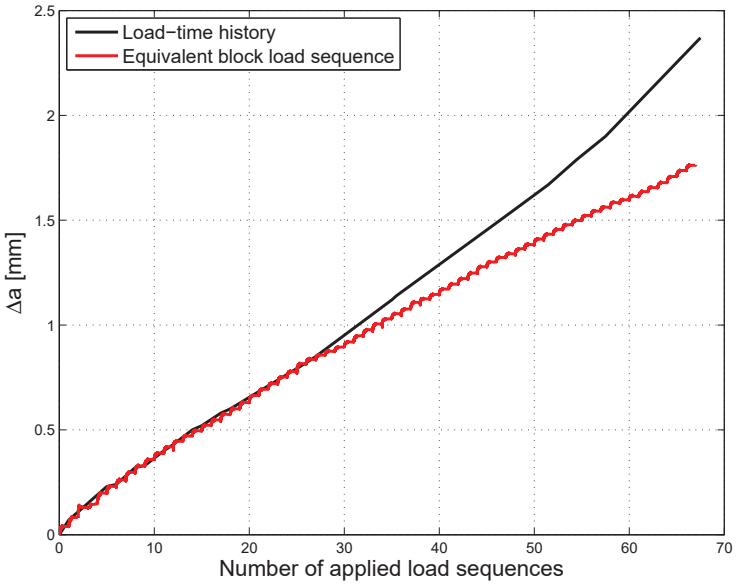

(a)

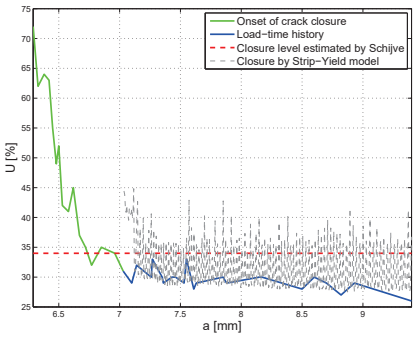

(b)

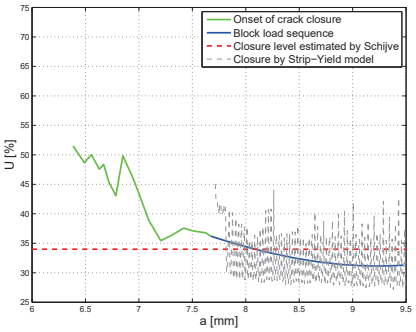

(c)

Figure 5: Experimental results of the tests carried out onto EA4T batch B specimens: a) comparison of crack propagation applying a load-time history or its equivalent block load sequence; b) crack closure measurements during the equivalent block load sequence test; c) crack closure measurements during the load-time history test.

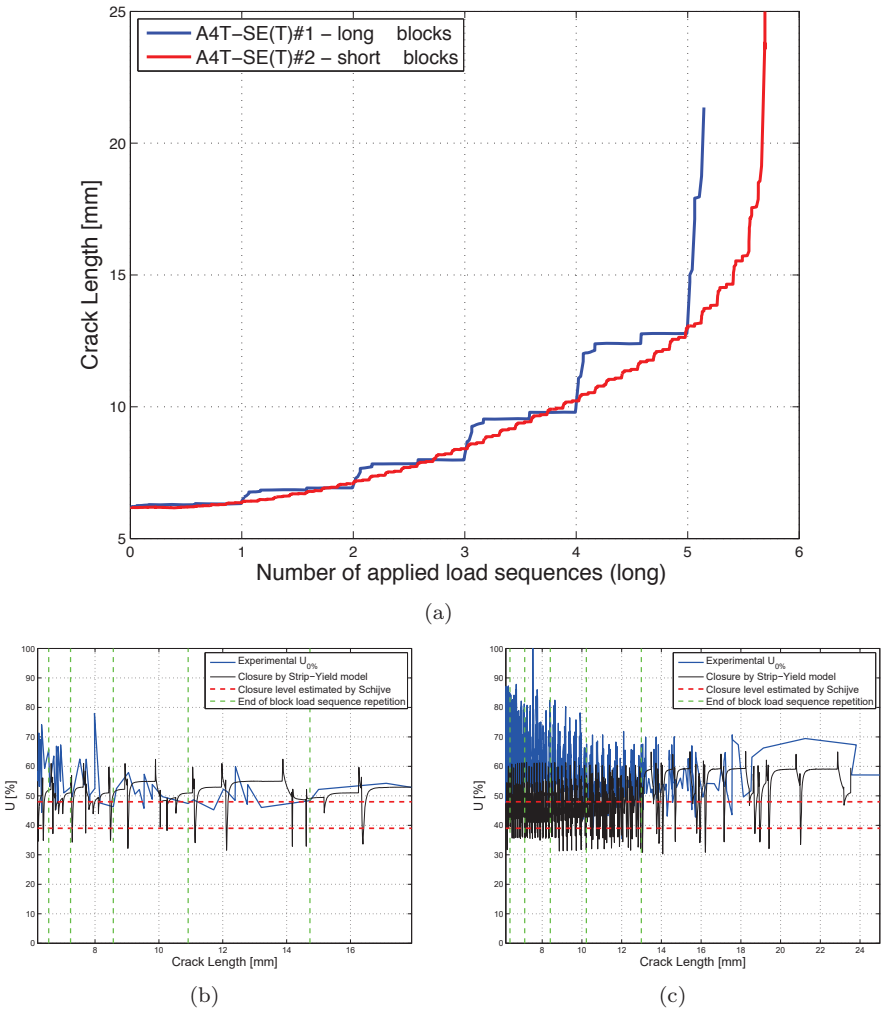

Figure 6: Experimental results of the tests carried out onto EA4T batch A specimens: a) comparison of crack propagation applying long and short blocks load sequences; b) crack closure measurements during the test with long blocks sequence; c) crack closure measurements during the test with short blocks sequence .

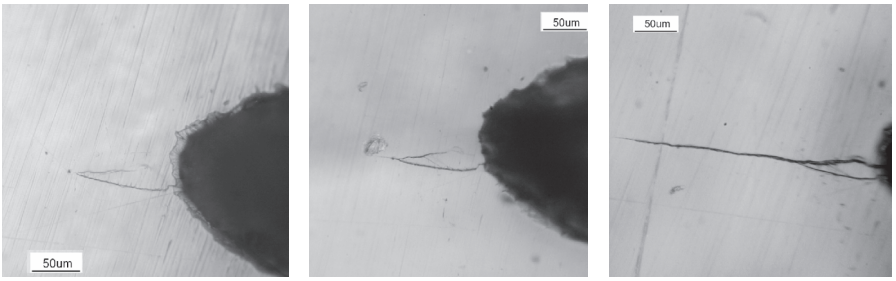

(a) end of crack stabilization (b) end of 100% block load sequence (c) end of 125% block load sequence

Figure 7: Example of surface crack growth; images of the plastic replicas captured by optical microscope at the same magnification.

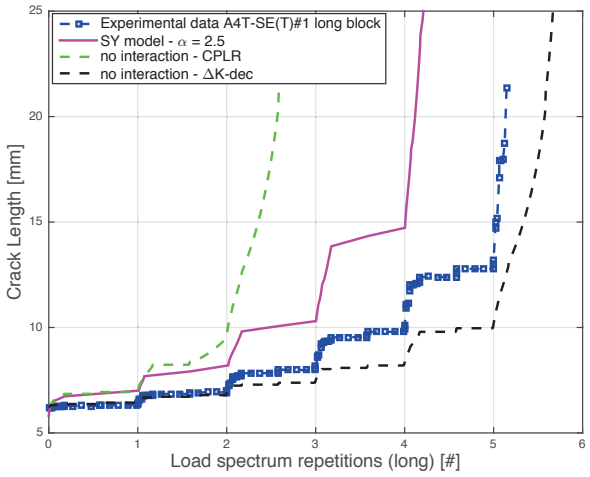

(a)

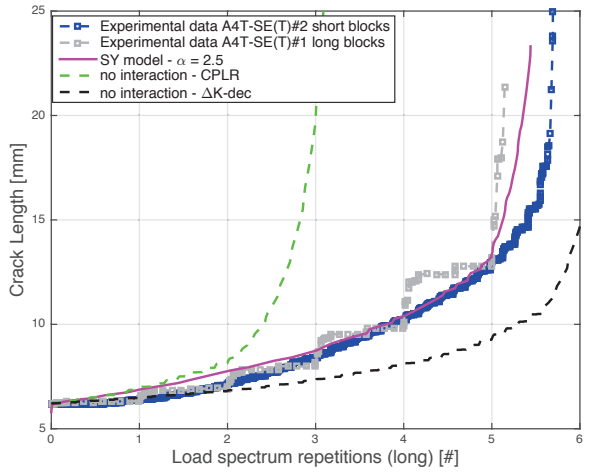

(b)

Figure 8: Crack growth simulations, by no-interaction and Strip Yield models, of the tests carried out onto EA4T batch A specimens: a) specimen A4T-SE(T)#1; b) specimen A4T-SE(T)#2.

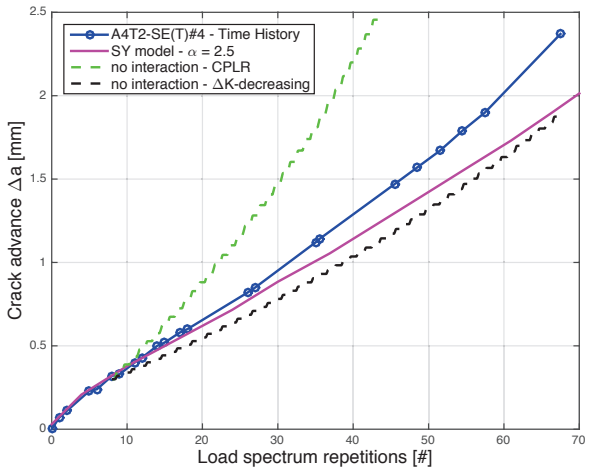

(a)

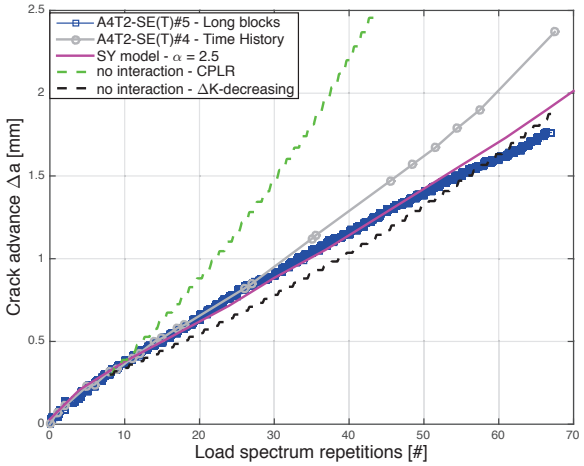

(b)

Figure 9: Crack growth simulations, by no-interaction and Strip Yield models, of the tests carried out onto EA4T batch B specimens: a) specimen A4T2-SE(T)#4; b) specimen A4T2-SE(T)#5.

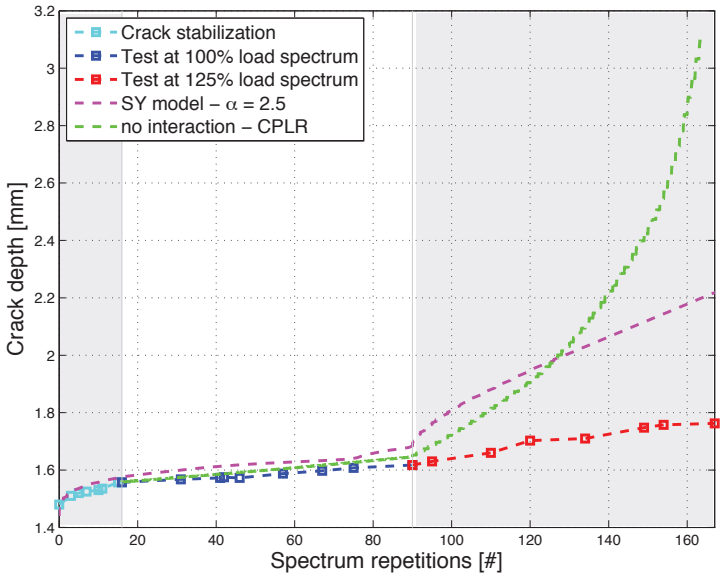

Figure 10: Experimental evidence and numerical simulations of the test carried out onto the full-scale specimen.

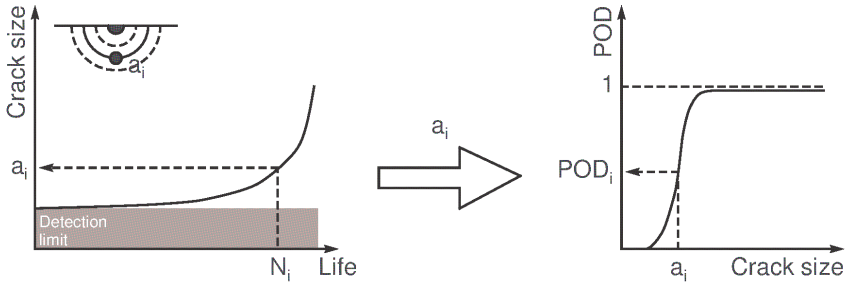

(a) determination of a single POD value (i_{th} inspection at N_i life)

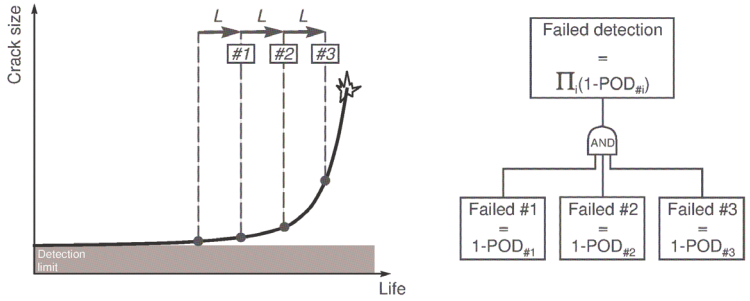

(b) total cumulative probability of non detection

Figure 11: Determination of inspection intervals and fault tree of an inspection procedure.

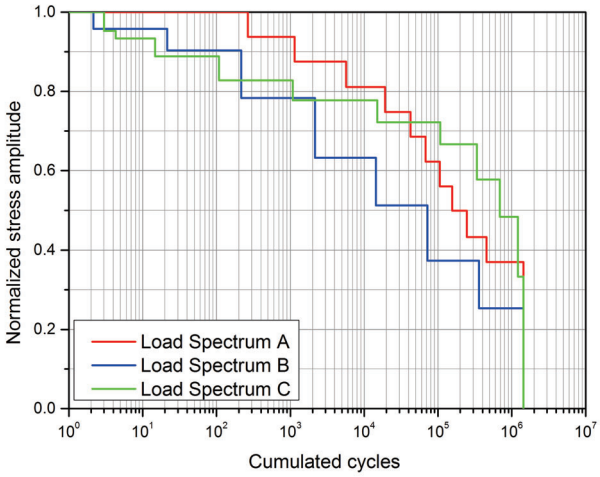

Figure 12: A comparison of the three load spectra for high speed train here considered: a) the spectrum adopted for VA tests; b) the HYPERWHEEL stress spectrum [29]; c) the WIDEM stress spectrum [12].